TURBULENCE SIMULATION VIA THE LATTICE-BOLTZMANN METHOD ON HIERARCHICALLY REFINED MESHES

3 authors, including:

Matthias Meinke
RWTH Aachen University
282 PUBLICATIONS **2,356** CITATIONS

European Conference on Computational Fluid Dynamics
ECCOMAS CFD 2006
P. Wesseling, E. Oñate and J. Périaux (Eds)

TURBULENCE SIMULATION VIA THE LATTICE-BOLTZMANN METHOD ON HIERARCHICALLY REFINED MESHES

R.K. Freitas*, M. Meinke, and W. Schröder

*RWTH Aachen University, Institute of Aerodynamics
Wüllnerstr. zw. 5 u. 7, 52062 Aachen, Germany
e-mail: R.Freitas@aia.rwth-aachen.de
web page: http://www.aia.rwth-aachen.de

Key words: Turbulence Simulation, Lattice-Boltzmann Method, Grid Refinement

Abstract. *In the present work the application of hierarchical grid refinement for the Lattice-Boltzmann Method (LBM) to simulate turbulent flows has been investigated. A transformation and interpolation scheme has been developed based on a volumetric approach, independent of a specific collision model and therefore, generally applicable to all variants of the LBM. Besides a short review of the LBM the developed scheme is presented. Furthermore, the validity of the method is demonstrated by solutions for Poiseuille, cavity, and turbulent channel flow.*

1 INTRODUCTION

The Lattice-Boltzmann Method (LBM) is based on the gas kinetic assumptions of the Boltzmann equation. It can be used to simulate continuum flows. The LBM is a competitive alternative to conventional Navier-Stokes based computational fluid dynamics (CFD) methods in several fields of application like e.g. multiphase flows and flows through porous media. The applicability of the method to simulate turbulent flows has been demonstrated in numerous publications.[1–4]

The original uniform grid based discretization of the LBM makes the method inappropriate for computations with varying resolution requirements, like the simulation of wall bounded turbulence. One possibility to tackle this problem is the application of hierarchical grid refinement techniques, which maintain the uniformity on each grid level while enabling the exchange between cells of different levels by applying proper interpolation and transformation algorithms.

In this study a grid refinement approach similar to that of Filippova and Hänel[5] is suggested. Unlike the approach in [5] a cell centered approach is used in the current study and the transformation and interpolation operations are formulated independent of the applied LBM scheme, allowing the application of arbitrary collision models.

In the following two sections a short review on the Boltzmann equation and the LBM will be given. In section 4 the refinement scheme is presented and validated in section 5. Section 6 describes the performed turbulence simulation and discusses the results followed by the conclusion and outlook in the last section.

2 BOLTZMANN EQUATION

The Boltzmann equation describes the evolution of a molecular distribution function in the so-called phase space, which is the superposition of an Euclidian space and a velocity space.

$$\frac{\partial f}{\partial t} + \sum_{i=1}^{3}(\xi_i \cdot \frac{\partial f}{\partial x_i}) + \sum_{i=1}^{3}(\frac{\partial f}{\partial \xi_i} \cdot \frac{F_i}{m}) = \int_{\xi_1'}\int_{A_C} (f'f_1' - ff_1)\ \vec{g}\ dA_c d\vec{\xi} \tag{1}$$

The quantity f is the particle distribution function, ξ_i and F_i represent the components of the molecular velocity vector and applied external force vector, respectively, and m denotes the mass. The variables f' and f_1' are the pre-collision values of a molecular distribution becoming post-collision values f and f_1 through collision.

In the following the external forces are assumed to be zero , thus the third term on the left-hand side disappears

$$\frac{\partial f}{\partial t} + \sum_{i=1}^{3}(\xi_i \cdot \frac{\partial f}{\partial x_i}) = \int_{\xi_1'}\int_{A_C} (f'f_1' - ff_1)\ \vec{g}\ dA_c d\vec{\xi}. \tag{2}$$

Macroscopic flow properties are obtained from the moments of the distribution function

$$\rho(t,\vec{x}) = \int_{-\infty}^{\infty} f(t,\vec{\xi},\vec{x}) d\vec{\xi} \tag{3}$$

$$\rho(t,\vec{x})u_i(t,\vec{x}) = \int_{-\infty}^{\infty} \xi_i f(t,\vec{\xi},\vec{x}) d\vec{\xi} \tag{4}$$

$$\rho(t,\vec{x})e = \int_{-\infty}^{\infty} f(t,\vec{\xi},\vec{x}) \frac{\xi_i^2}{2} d\vec{\xi}, \tag{5}$$

where ρ is the fluid density, ρu_i the momentum in the i-direction, and ρe the specific energy. The index i stands for the space dimension, i.e. $i = 1, 2, 3$.

2.1 Bhatnagar-Gross-Krook model

A simplified collision operator for the Boltzmann equation has been proposed by Bhatnagar, Gross and Krook[6] (BGK). In the BGK model the collision term of the Boltzmann equation is replaced by $\omega(F - f)$ resulting in

$$\frac{\partial f}{\partial t} + \xi_i \cdot \frac{\partial f}{\partial x_i} = \omega(F - f), \tag{6}$$

where ω represents the collision frequency and F is the local equilibrium distribution function

$$F(\vec{\xi}) = \frac{n}{(2\pi RT)^{3/2}} \cdot exp\left[-\frac{|\vec{\xi} - \vec{u}|}{2RT}\right] \tag{7}$$

with the specific gas constant R, the static temperature T, the particle density n, the molecular velocity components $\vec{\xi}$, and the macroscopic velocity vector $\vec{u}$.

The moments of (6) are the same as for the Boltzmann equation and the correspondence to the Navier-Stokes equations can be demonstrated through the Chapman-Enskog expansion,[7] which also gives the relation between collision frequency ω and kinematic viscosity ν

$$\omega(\nu, T) = \frac{c_s^2}{\nu}, \tag{8}$$

where $c_S = \sqrt{RT}$ is the isothermal speed of sound.

3 LATTICE BOLTZMANN METHOD

The LBM is based on the discretization of the phase space and a specialized discretization of the BGK equation.

3.1 Phase space discretization

In two dimensions the phase space is discretized with the D2Q9 model. The DnQm notation, in which n stands for the number of dimensions and m denotes the number of discrete velocities, has been introduced by Qian *et al.*[8] In figure 1 the phase space

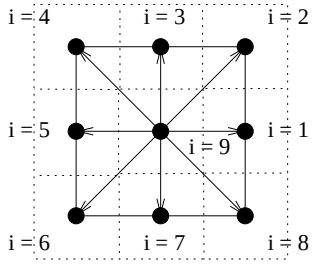

Figure 1: The D2Q9 model

discretization of the D2Q9 model is shown. The dotted lines represent the cell boundaries, while the arrows stand for the discrete velocities ξ_i

$$\xi_i = \xi_0 \cdot \begin{cases} (\pm 1, 0); (0, \pm 1) & i = 1..4 \\ (\pm 1, \pm 1) & i = 5..8 \\ (0, 0, 0) & i = 9. \end{cases} \tag{9}$$

For three dimensions the D3Q19 model has been applied

$$\xi_i = \xi_0 \begin{cases} (0,0,\pm 1);(0,\pm 1,0);(\pm 1,0,0) & i = 1..6 \\ (\pm 1,\pm 1,0);(\pm 1,0,\pm 1);(0,\pm 1,\pm 1) & i = 7..18 \\ (0,0,0) & i = 19. \end{cases} \tag{10}$$

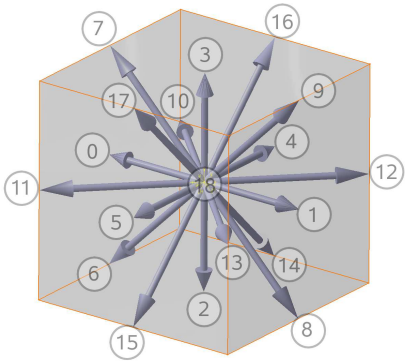

Figure 2: The D3Q19 model

3.2 Discrete BGK-equation

The LBM is a special discretization of equation (6), using first-order forward differences

$$\frac{f_{i+1}^{n+1} - f_{i+1}^{n}}{\Delta t} + \xi_i \frac{f_{i+1}^{n} - f_{i}^{n}}{\Delta x} = \omega(F - f_i^n). \tag{11}$$

By choosing $\xi_i = \frac{\Delta x}{\Delta t}$, i.e. using a fixed CFL number of 1, the above equation reduces to:

$$f_{i+1}^{n+1} = f_i^n + \Delta t \cdot \omega(F - f_i^n). \tag{12}$$

This formulation can be split into a collision and a propagation step

$$\tilde{f}_i^n = \Delta t \cdot \omega(F - f_i^n) \tag{13}$$

$$f_{i+1}^{n+1} = \tilde{f}_i^n. \tag{14}$$

Like for the continuous Boltzmann equation the macroscopic flow properties are moments of the distribution function

$$\rho = \sum_{i=1}^{i=i_{max}} f_i = \sum_{i=1}^{i=i_{max}} F_i \tag{15}$$

$$\rho u_\alpha = \sum_{i=1}^{i=i_{max}} \xi_\alpha f_i = \sum_{i=1}^{i=i_{max}} \xi_\alpha F_i \tag{16}$$

$$\rho(e + u_\alpha^2) = \sum_{i=1}^{i=i_{max}} \xi_\alpha^2 f_i = \sum_{i=1}^{i=i_{max}} \xi_\alpha^2 F_i \tag{17}$$

with the space dimension $\alpha = 1, 2, 3$. For the discrete formulation ω becomes

$$\omega(\nu) = \frac{\delta t c_S^2}{\nu + \delta t \cdot c_S^2/2}. \tag{18}$$

That is, the discrete collision frequency approaches the continuous collision frequency (8) in the limit $\delta t \to 0$, which also means for the lattice $\delta x \to 0$.

3.3 Discrete Maxwell equilibrium function

The discrete Maxwell equilibrium function F is obtained by Taylor expansion of equation (7) at Mach number zero and depends on the choice of the phase space discretization. It reads

$$F_i(\vec{r}, t) = \rho\ t_p\big[1 + \frac{\xi_{i,\alpha} u_\alpha}{c_S^2} + \frac{u_\alpha u_\beta}{2c_S^2}(\frac{\xi_{i,\alpha}\xi_{i,\beta}}{c_S^2} - \delta_{\alpha,\beta})\big] \tag{19}$$

where $\alpha = 1, 2, 3$ and $\beta = 1, 2, 3$ represent the space dimensions and

$$\delta_{\alpha\beta} = \begin{cases} 0 & \text{for } \alpha \neq \beta \\ 1 & \text{for } \alpha = \beta. \end{cases}$$

In equation (19) the summation is implied for repeated indices. The weighting factors t_P with p being the square modulus of the discrete velocities ξ_i are chosen such that macroscopic symmetry and conservation of mass and momentum are satisfied.[8] The different weighting factors are given in table 1.

Incompressible BGK model

The standard LBM describes weakly compressible flows. Since the Taylor series expansion of the Maxwell equilibrium distribution is performed at Mach number 0. To further decouple the pressure and the density, i.e., to obtain a solution method for incompressible flows a modified equilibrium distribution has been chosen as presented by Zou *et al.*[9] The modified equilibrium distribution reads

$$F_i(\vec{r}, t) = \ t_p\big[\rho + \frac{\xi_{i,\alpha} u_\alpha}{c_S^2} + \frac{u_\alpha u_\beta}{2c_S^2}(\frac{\xi_{i,\alpha}\xi_{i,\beta}}{c_S^2} - \delta_{\alpha,\beta})\big]. \tag{20}$$

Model	t_0	t_1	t_2	c_S^2
D2Q9	4/9	1/9	1/36	$1/3\ \xi_0^2$
D3Q19	1/3	1/18	1/36	$1/3\ \xi_0^2$

Table 1: Weighting factors for D2Q9 and D3Q19 model

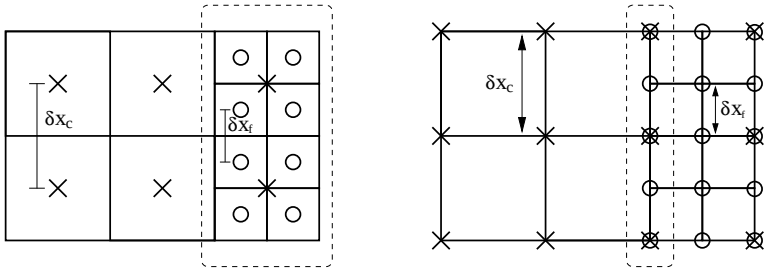

Figure 3: Cell centered (left) and node centered scheme (right). The circles and crosses represent the centers of the fine grid and coarse grid cells, respectively. The dashed line encloses the interface region.

4 GRID REFINEMENT SCHEME

The original uniform grid based discretization of the LBM is not the proper choice for computations with varying resolution requirements like, e.g., the simulation of wall bounded turbulence. This situation can be improved by applying hierarchically refined grids as has been proposed by several authors.[5,10–12] The introduction of local grid refinement leads to an inconsistency of neighboring relations on the boundary of a region, i.e., the nodes or cells of a certain level do not have a complete set of neighbors anymore. This leads to a lack of information either in the propagation or collision step of the standard LBM. A natural solution approach is to use the nearest neighbors from a different grid level to reconstruct the missing information, like it is common in the Finite Volume Method (FVM). Filippova and Haenel[5] have shown that such a reconstruction not only requires the interpolation of missing distributions from the different grid neighbors, but also requires a transformation of the non-equilibrium part of the distribution function depending on the grid level. Next, the interpolation used in this study will be discussed followed by a derivation of the developed transformation scheme.

4.1 Interpolation

The interpolation mainly depends on the chosen type of mesh, i.e., cell or node centered (figure 3). In the interface region, i.e., for the dashed box of the node centered grid, every second fine grid node coincides with a coarse grid point and thus needs no interpolation while the other fine grid nodes are interpolated from the two nearest and four next nearest neighbors on the coarse grid. The different treatment of the interface cells can lead to a

staggered solution, which is a common issue in LBM simulations. For the cell centered scheme all missing fine grid distributions at the interface are interpolated from the closest four or eight coarse grid cells. In this study the cell centered scheme has been applied and a nonlinear interpolation is used to calculate the missing distributions. In figure 4

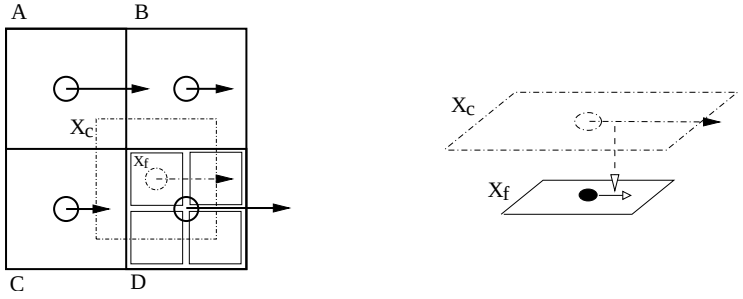

Figure 4: Bilinear interpolation (left) and transformation (right)

the cells $A - D$ are coarse grid cells and the centers of gravity of X_C and X_f have the same location. The missing distributions on the fine grid for X_f are obtained in two steps. First, the distributions of the virtual coarse grid cell X_C are calculated by bilinear (2D) or trilinear (3D) interpolation (figure 4, left). The second step is the transformation from X_C to X_F (figure 4, right), which will be described in the next subsection.

Assuming a maximum level difference of one between neighboring cells the distribution functions for X_C are

$$f_i(X_C) = \frac{1}{16} f_i(A) + \frac{3}{16} f_i(B) + \frac{3}{16} f_i(C) + \frac{9}{16} f_i(D) \tag{21}$$

The transfer to the three-dimensional case applies a trilinear interpolation

$$f_i(X_C) = \frac{1}{64}(3f_i(A)+9f_i(B)+9f_i(C)+27f_i(D)+1f_i(E)+3f_i(F)+3f_i(G)+9f_i(H)). \tag{22}$$

The interpolation from fine to coarse grids reduces to simple averaging of the fine grid cell distributions.

4.2 Transformation

The interpolation from the preceding subsection only provides the distributions for X_C, i.e., on the coarse grid. To obtain the distributions at X_F, i.e., on the fine grid, a transformation of the non-equilibrium part $f^{(1)}$ must be performed. Filippova and Hänel[5] have derived a formulation for the transformation between post collision distribution functions of different relaxation parameters ω based on the Chapman-Enskog expansion of the non-dimensional BGK-equation. In the following a similar approach will be taken, which provides formulations independent of the collision step. Using the

non-dimensional values:

$$\bar{x} = \frac{x}{L}, \qquad \bar{t} = t\frac{\xi_0}{L}, \qquad \bar{\omega} = \frac{\omega l_\mu}{\xi_0}, \qquad \bar{f} = f \cdot {l_\mu}^3, \qquad \bar{\xi}_i = \frac{\xi_i}{\xi_0} \tag{23}$$

inserting these into equation (6) the non-dimensional BGK equation reads either

$$\epsilon\big(\frac{\partial \bar{f}}{\partial \bar{t}} + \bar{\xi}_i \frac{\partial \bar{f}}{\partial \bar{x}}\big) = \bar{\omega}(\bar{f}^{eq} - \bar{f}) \qquad \text{with } \epsilon = l_\mu / L \mathrel{\hat{=}} Kn \tag{24}$$

or by introducing the substantial derivative

$$\epsilon \frac{Df}{Dt} = \omega(f^{eq} - f), \tag{25}$$

where the overbar has been neglected for clarity. Applying the Chapman-Enskog expansion (CEE)

$$f = f^{(0)} + \epsilon f^{(1)} + \epsilon^2 f^{(2)} \dots \tag{26}$$

in the limit of zero Knudsen number to equation (25) one obtains $f^{eq} = f^0$ and thus

$$f^{(1)}\omega = \big(\frac{\partial f^{(eq)}}{\partial t} + \xi_0 \frac{\partial f^{(eq)}}{\partial x_i}\big) \tag{27}$$

The right-hand side of this equation only depends on the equilibrium distribution, which in turn is a function of the macroscopic variables only and therefore, independent of the grid level. This gives a connection between distribution functions of different grid levels. Assuming a coarse grid and a fine grid distribution, the non-equilibrium parts are related by

$$\omega_F f_F^{(1)} = \omega_C f_C^{(1)}. \tag{28}$$

With the above relation and the CEE equation (12) can be formulated for a coarse grid distribution as a function of the fine grid distribution

$$\begin{aligned} f_C &= f^{(eq)} + \epsilon_C f_C^{(1)} \\ &= f^{(eq)} + \epsilon_C \frac{\omega_F}{\omega_C} f_F^{(1)} \\ &= f^{(eq)} + \epsilon_C \frac{1}{\epsilon_F}\frac{\omega_F}{\omega_C}(f_F - f^{eq}) \\ &= f^{(eq)} + n\frac{\omega_F}{\omega_C}(f_F - f^{eq}) \end{aligned} \tag{29}$$

with the scaling factor $n = \frac{\epsilon_C}{\epsilon_F} = \frac{\delta x_C}{\delta x_F}$ and vice versa

$$f_F = f^{(eq)} + \frac{1}{n}\frac{\omega_C}{\omega_F}(f_C - f^{eq}). \tag{30}$$

Note that the above formulation for the transformation is valid for the propagation as well as for the collision step. Furthermore, the derivation implies $Kn >> 1$ which corresponds to $\delta x << L$, i.e., if the grid resolution is too low, the above derivation becomes invalid. On the other hand, this is also true for the collapse of the Navier-Stokes equations of the basic LBM algorithm and therefore, imposes no additional constraint.

5 VALIDATION

A first validation of the above described grid refinement procedure is performed for the plane Poiseuille flow. The grid, which is refined in the vicinity of the upper and lower plate is shown in figure 5. The comparison of the numerical and the analytical velocity distribution shows the refinement to introduce no error.

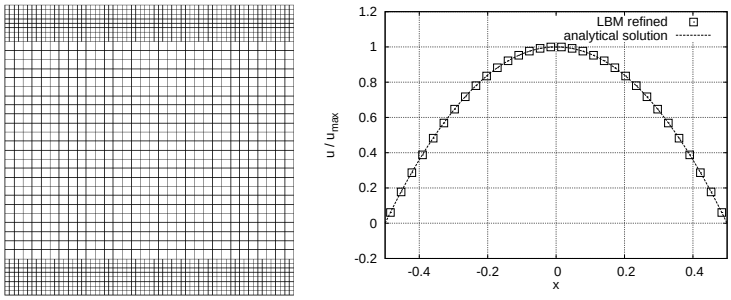

Figure 5: Grid for 2D-Poiseuille flow and velocity profile at Re=100

To verify that the smooth solution is not only due to the parallel alignment of the interface and the flow direction another problem with a more complex grid topology is simulated, i.e., the lid driven cavity flow at $Re = 500$. The refined mesh is given in figure 6. The streamlines of the refined and unrefined grids plotted in figure 7 show very good agreement for both simulations.

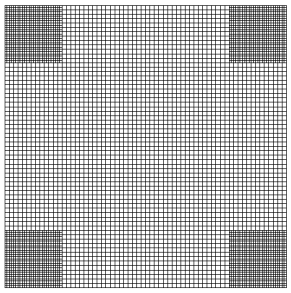

Figure 6: Refined grid for driven cavity flow

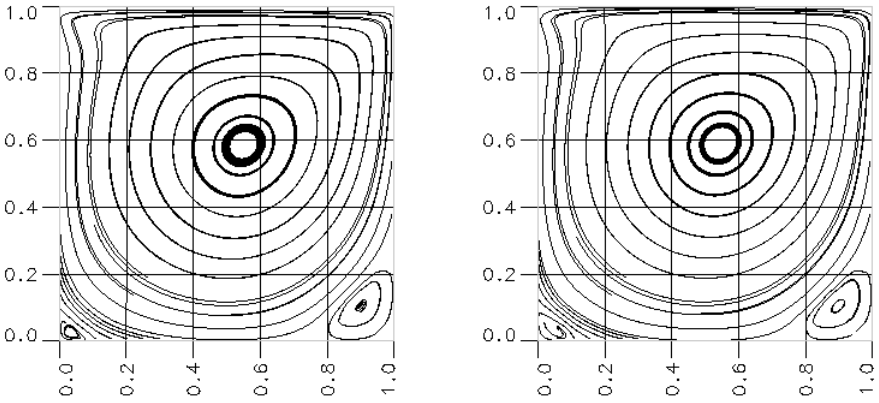

Figure 7: Streamlines for driven cavity at $Re = 500$ with for unrefined (left) and refined grid (right)

6 TURBULENCE SIMULATION

Next, turbulent channel flow is computed using refined meshes near the upper and lower wall as evidenced in figure 8. The computational domain of the channel flow possesses a streamwise, normal, and spanwise extension of $\pi H \times 2H \times 0.289\pi H$ according to the minimum specifications for a periodic channel given by JIMÉNEZ & MOIN.[13] The simulation is performed for a Reynolds number based on the skin friction velocity and the channel halfwidth H Re_τ of 180, which corresponds to a Reynolds number based on the bulk velocity of $R_H = 3800$. The resolution of the base grid is $128 \times 64 \times 32$ cells. The mesh near the walls is refined by one level up to a normal distance in inner coordinates of approximately 55. The total number of cells is 917,504, which is less than half of the 2,097,152 cells that are necessary for a completely uniform grid with the same resolution. In the refined region a $y^+ = 2.8125$ is obtained, while in the center of the channel the value of y^+ is 5.625. Since the walls are located directly on the cell boundaries y^+ at the walls is 1.40625.

The turbulent character of the flow simulation is evidenced by the velocity contours in figure 9. A more quantitative result is obtained by the average velocity profile. The numerical velocity distribution and the log law curve almost collapse. However, a closer look reveals an error being introduced at the interface between the coarse and fine grid. This behavior is due to the fact that the resolution of the coarse grid is already very close to the stability limit for the given Reynolds number, i.e., the formerly mentioned small Knudsen number condition is violated.

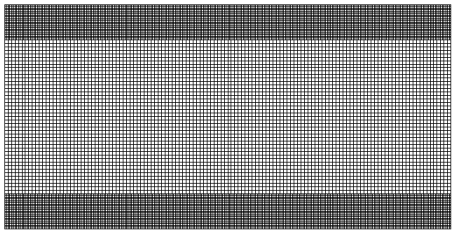

Figure 8: Refined grid for periodic channel flow

7 CONCLUSION AND OUTLOOK

In this study a grid refinement approach for the LBM based on the transformation procedure by HÄNEL AND FILIPPOVA in conjunction with a respectively, bilinear and trilinear interpolation has been introduced. The formulation of the transformation is independent of the applied LBM scheme and can be applied in the propagation as well as in the collision step. The method has been successfully applied to compute Poiseuille, cavity flow, and wall-bounded turbulence. However, the results show the grid refinement to influence the channel flow solution. Simulations with a higher grid resolution, which are

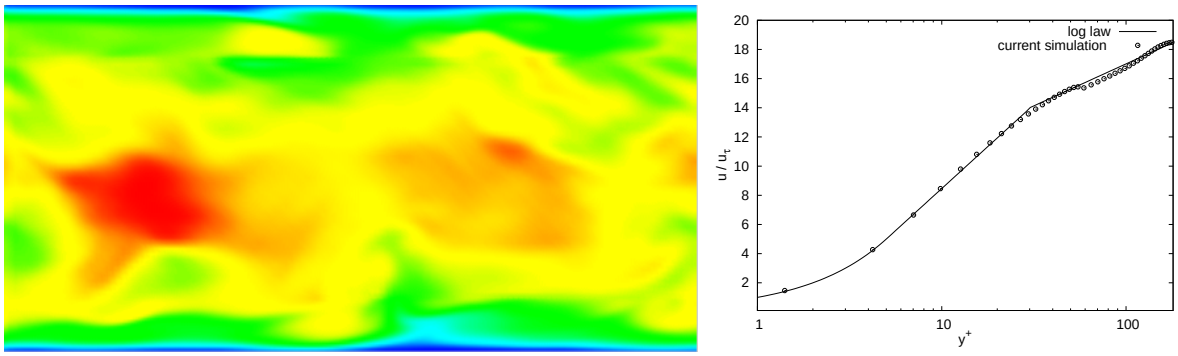

Figure 9: Velocity contours of instantaneous flow field (left) and logarithmic profile (right)

currently performed, will clarify whether or not this is mainly due to too low a resolution of the coarse grid region.

Furthermore, the Reynolds stress tensor and the impact of different interpolation schemes on the accuracy of the simulation will be analyzed in detail in future investigations.

REFERENCES

[1] P. Lammers, K. N. Beronov, G. Brenner, and F. Durst. Direct Simulation with the Lattice Boltzmann of Developed Turbulence in Channel Flows. *High Performance Computing in Science and Engineering*, pages 43–58, 2002.

[2] H. Yu, L. S. Luo, and S. S. Girimaji. MRT Lattice Boltzmann Equation Implementation for LES of Turbulence: Computation of Square Jet Flow. *to be published in Computers and Fluids*, 2005.

[3] H. Yu, S. S. Girimaji, and L. S. Luo. Lattice Boltzmann simulations of decaying homogeneous isotropic turbulence. *Phys. Rev. E*, 71, 2005.

[4] M. Krafczyk, J. Tölke, and L. S. Luo. Large-Eddy Simulations with a Multiple-Relaxation-Time LBE Model. *Int. J. Mod. Phy. B*, 17:33–39, 2003.

[5] O. Filippova and D. Hänel. Grid Refinement for Lattice-BGK Models. *J. Comput. Physics*, 147:219–228, 1998.

[6] P. L. Bhatnagar, E. P. Gross, and M. Krook. A Model for Collision Processes in Gases. I. Small Amplitude Processes in Charged and Neutral One-Component Systems. *Phys. Rev.*, 94(3):511–519, 1954.

[7] D. Hänel. *Molekulare Gasdynamik*. Springer, 2004.

[8] Y. H. Qian, D. D'Humieres, and P. Lallemand. Lattice BGK Models for Navier-Stokes Equation. *Europhysics Letters*, 17(6):479–484, 1992.

[9] Q. Zou, S. Hou, S. Chen, and G. D. Doolen. An improved incompressible Lattice Boltzmann model for time-independent flows. *J. Stat. Phys.*, 81:35, 1996.

[10] M. Krafczyk. *Gitter-Boltzmann-Methoden: Von der Theorie zur Anwendung.* TU Braunschweig, 2001. Habilitationsschrift.

[11] D. Yu, R. Mei, and W. Shyy. A multi-block lattice boltzmann method for viscous fluid flows. *Int. J. Numer. Meth. Fluids*, 39:99–120, 2002.

[12] M. Rohde, D. Kandhai, J.J. Derksen, and H.E.A. van den Akker. A generic, mass conservative local grid refinement technique for lattice-Boltzmann schemes. *Int. J. Numer. Meth. Fluids (in press)*, 2006.

[13] J. Jiménez and P. Moin. The minimal flow unit in near wall turbulence. *J. Fluid Mech.*, 225:213–240, 1991.